

# Experimental Asynchronous Measurement-Device-Independent Quantum Cryptographic Conferencing

Yifeng Du<sup>1</sup>, Yang Hu<sup>1</sup>, Yufeng Liu<sup>1</sup>, Wenhan Yan<sup>1</sup>, Jinghao Zhang<sup>1</sup>, Shining Zhu<sup>1</sup>, and Xiao-Song Ma<sup>1,2,3,\*</sup>

<sup>1</sup>National Laboratory of Solid State Microstructures,

School of Physics, College of Engineering and Applied Sciences,

Collaborative Innovation Center of Advanced Microstructures, Jiangsu Physical Science Research Center  
Jiangsu Key Laboratory of Quantum Information Science and Technology, Nanjing University, Nanjing 210093, China

<sup>2</sup>Synergetic Innovation Center of Quantum Information and Quantum Physics,

University of Science and Technology of China, Hefei, 230026, China

<sup>3</sup>Hefei National Laboratory, Hefei 230088, China

The quantum cryptographic conferencing (QCC) protocol, which distributes identical secure keys to user groups, is a crucial component of the quantum network. Previous experimental works have implemented the measurement-device-independent (MDI) QCC, of which the key rate in an  $N$ -user network scales down as  $R \sim O(\eta^N)$ , respectively. Building on the MDI QCC protocol, the asynchronous MDI (AMDI) QCC protocol theoretically integrates the mode pairing scheme into QCC, significantly boosting the key rate to  $R \sim O(\eta)$ , which is independent of the number of users, and thus demonstrating greater application potential. Experimentally, in this work, we implement the three-user AMDI QCC network without global phase tracking by adopting the fast Fourier transform-based frequency difference estimation and the phase drift compensation technique. Finally, we achieve a key rate of about  $4.470 \times 10^{-9}$  bits per pulse under a maximum overall loss of about 59.6 dB. This work provides a scalable solution for the development of large-scale quantum communication networks in the future.

## INTRODUCTION

Quantum network (QN) aims to connect users through quantum communication protocols[1, 2]. Founded on the fundamental principles of quantum mechanics, quantum networks offer advantages that are unattainable with classical communication. They can operate in parallel with the traditional Internet, thereby enhancing communication performance. Within this promising blueprint, the quantum key distribution (QKD) protocol [3–8] endowed with the property of information-theoretic unconditional security serves as a critical component. Traditional point-to-point QKD protocols between two users have achieved substantial progress and development both theoretically [9–17] and experimentally [18–21], moving toward real-world practical application. Meanwhile, the research on multi-user QKD networks develops rapidly [22–25]. Building on this foundation, the quantum cryptographic conferencing (QCC) protocol, also known as quantum conference key agreement (QCKA) protocol [26–28], which extends two-user secure communication to multi-user scenarios, is key to further expanding the scale of quantum communication networks and improving their functionality.

QCC protocols distribute secure keys among communicating users via genuine multipartite entanglement states [29–31]. To date, the QCC protocols proposed theoretically can be categorized into entanglement-based (EB) protocols [32, 33] and time-reversal protocols [34–42]. In EB protocols, a source generates multi-photon entanglement states and transmits them to users for measurement. Previous relevant experimental work has realized

a four-user QCC communication network by preparing four-photon GHZ states [43], and six-photon graph states with more complex entanglement structures [44]. However, the complexity and low generation rate of multi-photon entanglement sources limit the practicality of EB protocols.

Time-reversal protocols, by contrast, establish quantum correlations among users through projective measurement of genuine multipartite entanglement states. Some of these protocols possess the measurement-device-independent (MDI) property, which makes them immune to all attacks targeting the detection node and thus ensures higher security. Furthermore, the user-node and detection-node of MDI QCC systems are compatible with mature MDI QKD systems, making the MDI QCC protocol easier to implement in practical applications. Theoretically, various MDI QCC protocols have been successively proposed, including polarization-encoding protocol [34], phase-matching protocol [36], asynchronous MDI (AMDI) protocol [41], multi-field protocol [42], and W-state-based protocols [35, 40]. In particular, the AMDI QCC protocol extends the idea of mode pairing from QKD to QCC, improving the original MDI QCC protocol, which requires multiphoton coincidence counting, into a single-photon protocol capable of breaking the PLOB bound [45] with a key rate of  $R \sim O(\eta)$ . Meanwhile, the AMDI QCC also eliminates the need for complex phase tracking technology. In terms of experimental research, recent works have successfully implemented the three-user polarization encoding MDI QCC network [46, 47], verifying the feasibility of the original protocols. Nevertheless, the low multiphoton coincidence counting rate under high channel loss restricts the large-scale ap-

plication of these protocols.

Building on previous works of MP QKD [48–53] and MDI QCC [46, 47], in this work, we construct a three-user communication network and successfully implement the AMDI QCC protocol [41] without global phase locking. Through the fast Fourier transform (FFT)-based frequency difference [51–54] estimation and the phase drift post-compensation technique for the multipath interferometer, we achieve a secure key rate of about  $3.940 \times 10^{-8}$ ,  $3.937 \times 10^{-8}$  and  $4.470 \times 10^{-9}$  bits per pulse (bpp) with a overall system loss of three users of about 39.3, 48.6 and 59.6 dB. Compared to the MDI QCC experiments [46, 47], our work significantly increases the overall loss tolerance of the communication system by more than 30 dB and enhances the communication distance and secure key rate of the MDI QCC protocol through a simple approach. Our work not only experimentally validates the feasibility of asynchronous mode-pairing schemes in multiuser quantum communication but also paves the way for the practical implementation of future large-scale quantum networks.

## PROTOCOL

In the  $N$ -user AMDI QCC protocol, each user  $U_i$  independently prepares a phase-randomized coherent state  $|\sqrt{k_i}e^{i\varphi_i}\rangle$ , where the coherent state intensity  $k_i$  is randomly selected from the signal state  $\mu$ , decoy state  $\nu$  and vacuum state  $o$ ;  $\varphi_i$  denotes a random phase. The optical pulses are sent by users to the detection node, where each pulse interferes with the pulse from the adjacent user at the beam splitters. If there is exactly one detector response within the time window, the detection node records and publicly announces information including the single-count event and the responding detector. Following multiple repetitions of the above process, users pair the single-count events from  $N$  detectors of different branches. Based on the corresponding total intensity  $k_i^{\text{tot}} = k_i^e + k_i^l$  and encoded random phase difference  $\theta_i = \varphi_i^l - \varphi_i^e$  of the paired early and late pulses announced by users, they determine the encoding basis and bit value, and calculate the corresponding quantum bit error rate (QBER). Specifically, the pairs with  $k_i^{\text{tot}} = \mu$  will be assigned to Z-basis events for key distillation, and the events with  $k_i^{\text{tot}} = 2\nu$  and the total encoding phase difference of all users  $\sum_{i=1}^N \theta_i \bmod 2\pi = 0$  or  $\pi$  will be assigned to X-basis. A secure conference key can be obtained after estimating parameters via the decoy-state method and performing classical post-processing [41].

For a communication network with  $N = 3$  users, the final secure key length under finite size is given by [41]:

$$L_{\min} = \underline{Y}_{111}^Z [1 - H_2(\bar{\epsilon}_{111}^{PZ})] - \max[H_2(e_{AB,AC,BC}^Z)] f n_Z - \log_2\left(\frac{4}{\epsilon_{\text{cor}}}\right) - 2 \log_2\left(\frac{2}{\epsilon' \hat{\epsilon}}\right) - 2 \log_2\left(\frac{1}{2\epsilon_{\text{PA}}}\right) \quad (1)$$

where  $\underline{Y}_{111}^Z$  and  $\bar{\epsilon}_{111}^{PZ}$  is pairing count and phase error rate of single-photon component of Z-basis pairs, respectively;  $e_{AB,AC,BC}^Z$  is Z-basis QBER between user AB, AC, and BC;  $n_Z$  is total pair counts of Z-basis pairs;  $f$  is the error correction efficiency;  $\epsilon_{\text{cor}}$ ,  $\epsilon'$ ,  $\hat{\epsilon}$  and  $\epsilon_{\text{PA}}$  are security parameters;  $H_2(x) = -x \log_2 x - (1-x) \log_2 (1-x)$  is the binary Shannon entropy function.

## EXPERIMENTAL SETUP

The experimental setup of the three-user communication network constructed in this work is illustrated in the Fig. 1. In the user nodes, three independent free-running continuous-wave (CW) lasers with a central wavelength of about 1536.61 nm and a nominal linewidth of less than about 1 kHz are used as the light source. In the encoder section, each user first employs three cascaded electro-optic intensity modulators (IMs) to modulate the continuous light into an optical pulse series with a repetition frequency of 250 MHz and a pulse width of about 260 ps in the key generation experiments. Each complete pulse sequence contains 5000 reference light pulses with the same intensity as the signal state and 39890 quantum light pulses for key generation. Besides, there is a recovery region of about 20  $\mu\text{s}$  between the reference pulses and the quantum pulses. In the phase encoding process following optical pulse generation, each user implements discrete random phase encoding with the slice number of  $M = 16$  using two electro-optic phase modulators (PMs), i.e.,  $\varphi_i = 2\pi M_i/M$ , where  $M \in \{0, 1, \dots, 15\}$ . Specifically, users apply electrical signals with amplitudes  $\{0, V_\pi\}$  to the first phase modulator, and electrical signals of the same pulse width with amplitudes  $\{0, V_{\pi/8}, \dots, V_{7\pi/8}\}$  to the second phase modulator. The pulse width of the electrical signals for phase modulation is about 1 ns.

After completing the encoding process, users filter the optical pulses with dense wavelength-division multiplexers (DWDMs), attenuate them to the single-photon level, and simulate fiber link losses using variable attenuators (VOAs) when transmitting the pulses to the detection node. Then the fiber polarization controllers (FPCs) and polarization-maintaining fiber polarization beam splitters (PMPBSs) work in coordination to align their polarization states to match. In the interferometer, the input light is first split into two parts by a  $1 \times 2$  polarization-maintaining beam splitter (PMBS), and each part is interfered with photons from the other two users at a  $2 \times 2$  PMBS, respectively. The split ratio of all beam splitters in the interferometer is 50:50. Superconducting nanowire single-photon detectors (SNSPDs) are employed to detect the output photons of the interferometer, exhibiting an average dark count rate of about 42 Hz. Finally, a time-to-digital converter (TDC) is used to record the time tag and channel of the detection events.

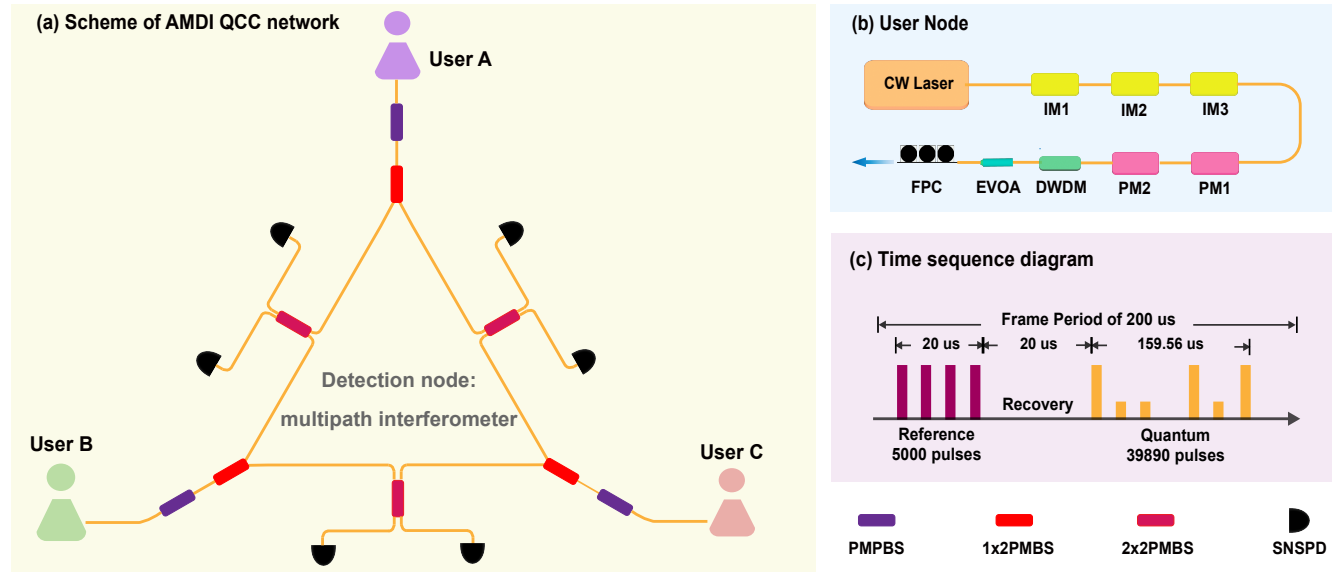


FIG. 1. Experimental setup of asynchronous measurement-device-independent quantum cryptographic conferencing (AMDI QCC). (a) Scheme of AMDI QCC network. The user transmits the encoded pulses to the multipath interferometer at the detection node for measurement. (b) The user node. Each user employs an independent free-running laser as the light source. The encoder section consists of cascaded three intensity modulators and two phase modulators, which perform decoy state and 16-slice random phase modulation, respectively. (c) The time sequence diagram of pulses prepared by users. The complete pulse sequence comprises the reference pulses for frequency difference and interferometer phase drift estimation, the quantum pulses for key generation, and the recovery region between reference and quantum pulses. Abbreviation of the components: BS, beam splitter; IM, intensity modulator; PM, phase modulator; DWDM, dense wavelength division multiplexer; VOA, variable optical attenuator; FPC, fiber polarization controller; PMPBS, polarization-maintaining polarization beam splitter; PMBS, polarization-maintaining beam splitter; SNSPD, superconducting nanowire single-photon detector.

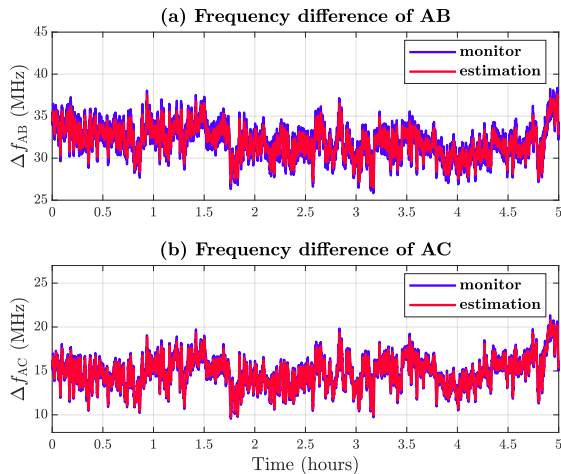


FIG. 2. Frequency differences estimation test results and beating frequency measurement results between (a) users AB, and (b) users AC in 5 hours.

## ESTIMATION OF FREQUENCY DIFFERENCES

In AMDI QCC, the sifting and key mapping of X-basis pairs depend on the encoding phase difference between paired early and late pulses. However, in the experiment

with independent free-running lasers, the frequency differences between the light sources introduce an additional phase difference that needs to be estimated and compensated for the paired pulses to decrease X-basis QBER. In the experiment, we pair reference pulses pairwise according to the method described in the MP QKD protocol and analyze the spectrum of the X-basis QBER using the FFT algorithm to estimate the frequency differences between the two users every about 0.4 seconds [51–54]. As shown in Fig. 2, in the test, we estimate the frequency difference about every 0.4 seconds and monitor the beating frequency between users AB and BC via an oscilloscope over a period of about 5 hours as a comparison. The results indicate that the estimation values are in good agreement with the measured values, demonstrating that our method can accurately estimate frequency differences. Based on the estimated frequency difference and the time interval between paired single counts, we can calculate the corresponding phase shift compensation value  $\theta_{\Delta f}$  by the method given in the Supplemental Material in detail [55].

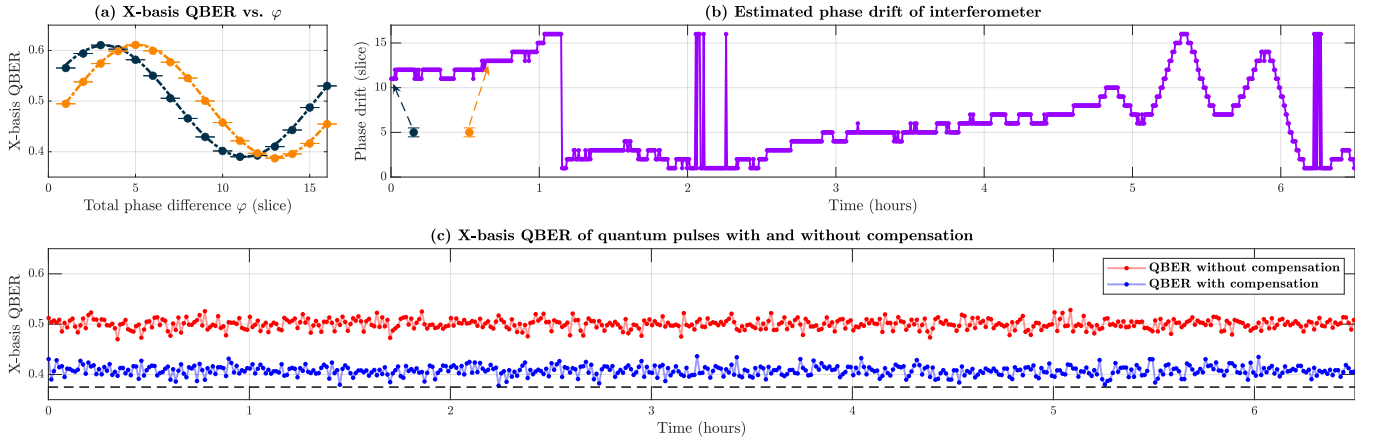


FIG. 3. Phase drift compensation and X-basis QBER. (a) Relationship between the X-basis QBER of the reference pulses and the total phase difference of the paired pulses after frequency difference compensation. The visibility of GHZ-HOM interference obtained by fitting the experimental data is about 0.22. The horizontal shift between the dark blue and orange cosine curves measured with a time interval of approximately 1000 seconds in the figure indicates the drift of the additional phase  $\Delta\varphi$ . (b) Estimated phase drift of the interferometer. We regard the phase slice value corresponding to the minimum QBER point in the figure (b) as the phase shift estimation value. In the calculations, we compute the phase values within the range of 0 to  $2\pi$ , and thus an abrupt change occurs in the phase shift values when the phase exceeds this range. (c) X-basis QBER of quantum pulses with and without compensation. After compensating the frequency difference and phase drift in the test, the X-basis QBER is reduced from about 50.02% to about 40.76%, with a theoretical minimum value of about 37.50% (black dashed line).

### POST-COMPENSATION OF PHASE DRIFT

On the other hand, the inherent phase drift of the multipath interferometer also has a significant impact on the X-basis QBER. Ideally, suppose that the total phase difference of the paired pulses including the total encoding phase difference  $\sum_{i=1}^N \theta_i$  and the phase shift  $\theta_{\Delta f}$  introduced by frequency difference is  $\varphi$ , then the X-basis QBER will be  $E_X = (1 - V \cos \varphi)/2$ , where  $V$  is the visibility of three-photon GHZ-HOM interference as shown in Fig. 3(b) [47]. As the filter criteria for the X-basis pairs, when  $\varphi = 0$  or  $\pi$ , the QBER reaches its extremum. However, in practice, there is a relative phase between two sub-pulses generated by the  $1 \times 2$  BSs in the interferometer, which introduces an additional phase shift  $\Delta\varphi$ , resulting in the QBER becoming  $E_X = [1 - V \cos(\varphi - \Delta\varphi)]/2$ . The additional phase shift  $\Delta\varphi$  in the all-fiber interferometer is prone to rapid drifting due to environmental disturbances, which causes the long-term average X-basis QBER to approach 50%. To solve this problem, in the experiment, we place the interferometer in an insulated box to maintain its phase relatively stable for over 20 seconds and compensate for the phase drift of the interferometer during post-processing. We perform three-photon pairing on the reference pulses after compensating for the frequency difference, and regard the phase slice value  $\theta_{\min}$  corresponding to the minimum QBER as the phase drift estimation value. During the key mapping process in the protocol, considering the phase drift of the interferometer, we adjust the filter criteria determining the X-basis pair to  $(\sum_{i=1}^N \theta_i + \theta_{\Delta f})$

$\text{mod } 2\pi \in \{\theta_{\min}, \theta_{\min} + \pi\}$ . In the experiment, we perform the above process about every 20 seconds. As shown in Fig. 3(c), by combining frequency difference estimation and phase drift post-compensation of the interferometer, we reduce the X-basis QBER of the reference pulses from about 49.80% to about 39.14%, while simultaneously reducing the X-basis QBER of the quantum pulses from about 50.02% to around 40.76%

### KEY GENERATION RESULTS

We perform key generation experiments under conditions with the all-user overall loss containing insertion loss and efficiency of detectors of about 39.3, 48.6 dB, and 59.6 dB. In the above cases, we accumulate about  $5 \times 10^3$ ,  $2 \times 10^4$ , and  $8 \times 10^4$  seconds of data, respectively. The encoding parameters used in the experiment are set as  $\mu = 0.286$ ,  $\nu = 0.026$ ,  $p_\mu = 0.1008$ ,  $p_\nu = 0.5398$ , and the maximum pairing time interval  $t_{\max} = 3 \mu\text{s}$ . The final secure key rates are about  $3.940 \times 10^{-8}$ ,  $3.937 \times 10^{-8}$  and  $4.470 \times 10^{-9}$  bpp with an overall loss of about 39.3 dB, 48.6 dB and 59.6 dB for each user, respectively. The key generation results in this work and other relevant works are shown in the Fig. 4. Compared with the previous MDI QCC experimental work [46, 47], the system's tolerable channel loss and secure key rate have been significantly improved from 21.5 dB to about 59.6 dB without a noticeable increase in experimental complexity.

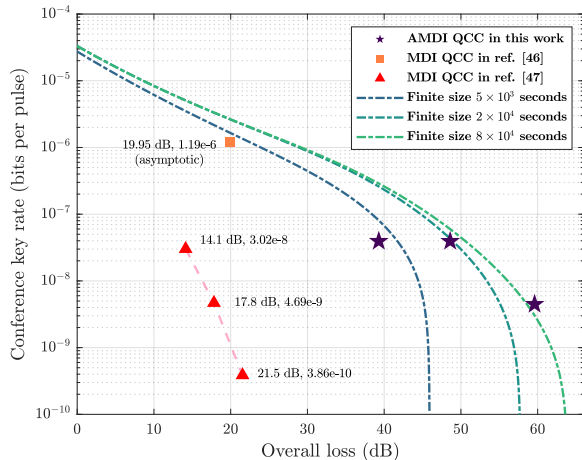


FIG. 4. Key generation results of the AMDI QCC in this work, and MDI QCC in [46, 47]. The dashed curves in the figure represent theoretical key rates corresponding to scenarios with data accumulation time of about  $5 \times 10^3$ ,  $2 \times 10^4$ , and  $8 \times 10^4$  seconds, respectively. The parameters used in the simulation are given in the Supplemental Material. For comparison, the experimental results of the prior works cited in the figure are calculated based on the data provided in those references.

## DISCUSSION

In this work, we have successfully implemented the AMDI QCC protocol without global phase tracking. Ideally, the key rate of the AMDI QCC protocol in the N-

user network scales down as  $R \sim O(\eta)$ , which is independent of the number of users and thus provides a more scalable scheme for the multiuser quantum network. Benefiting from the theoretical advancements of the protocol, the communication distance of the system in this work has been greatly improved compared with the previous experimental works on the MDI QCC protocol [46, 47]. With the rapid development of related technologies such as on-chip integrated multi-wavelength light sources [56–61], modulators [62] and detectors [63], it is expected that in the future, we can realize intercity quantum multi-party communication with a distance from single user node to detection node exceeding 100 km over optical fiber links, and lay a solid foundation for the realization of large-scale and scalable quantum networks.

*Note Added.*—During the final stage of this work, we became aware of a related experimental work on realizing phase-matching QCC [64], in which the performance of phase-matching QCC in symmetric and asymmetric fiber channels has been systematically studied.

## ACKNOWLEDGMENT

This research was supported by the Natural Science Foundation of Jiangsu Province (Grants No. BK20240006 and BK20233001), Quantum Science and Technology-National Science and Technology Major Project (Grants No. 2021ZD0300700 and 2021ZD0301500), and Nanjing University-China Mobile Communications Group Co., Ltd. Joint Institute.

## SUPPLEMENTAL MATERIALS

## S1 PAIRING ALGORITHM OF AMDI QCC IN THE EXPERIMENT

**Algorithm 1:** Pairing Algorithm of AMDI QCC in the experiment

---

**Input:** The set  $S = \{E_1, E_2, \dots, E_N\}$  of effective single-click events, where the  $i$ th event  $E_i = \{C_i, T_i\}$  has properties  $C_i$  (the detector channel) and  $T_i$  (the click time); maximum pairing time  $t_{\max}$

**Output:** The set  $P = \{P_1, P_2, \dots\}$  of pairing events, where the  $j$ th pair  $P_j = \{p_1^j, p_2^j, \dots, p_n^j\}$  consists of single-click events from  $n$  different branches.

- 1 Initialization: loop index  $i = 1$ ; iterate starting index  $k_{\text{start}} = 1$ ; temporarily unpaired events index  $k_{\text{pairing}} = N$  and  $k_{\text{unpairing}} = N$ ; pair number index  $k_p = 1$ ; temporary empty register set  $A$ ; the number of events in the register  $n_{\text{temp}}$ ;
- 2 **while**  $i < N - 1$  **do**
- 3     **for**  $j = k_{\text{start}}$  **to**  $N$  **do**
- 4         identify click branch  $B_j$  from click detector channel  $E_j.C_j$ ;
- 5         **if**  $j = k_{\text{start}}$  **then**
- 6             append the event  $E_j$  into  $A$ :  $A[B_j] = E_j$ ;
- 7             set starting timetag:  $t_{\text{start}} = E_j.T_j$
- 8         **else**
- 9             **if**  $A[B_j] = \emptyset$  **then**
- 10                 **if**  $E_j.T_j - t_{\text{start}} \leq \Delta t_{\max}$  **and**  $j < N$  **then**
- 11                     append the event  $E_j$  into  $A$ :  $A[B_j] = E_j$ ;
- 12                     set temporarily unpaired events index:  $k_{\text{pairing}} = \min[k_{\text{pairing}}, j]$ ;
- 13                     count the number of events in the register:  $n_{\text{temp}} = n_{\text{temp}} + 1$ ;
- 14                     **if**  $\emptyset \notin A[k_p]$  **then**
- 15                         append the single counts pair  $A$  into set  $P[k_p]$ ;
- 16                         update the corresponding pair index:  $k_p = k_p + 1$ ;
- 17                         set new iterate starting index  $k_{\text{start}} = \min[j + 1, k_{\text{unpairing}}]$ ;
- 18                         set new loop index  $i = k_{\text{start}}$ ;
- 19                         re-initialize the temporarily unpaired events index  $k_{\text{pairing}} = N$ ,  $k_{\text{unpairing}} = N$ , temporary empty register set  $A$ , and the number of events in the register  $n_{\text{temp}}$ ;
- 20                         **break**;
- 21                     **end**
- 22             **else**
- 23                 **if**  $n_{\text{temp}} = 1$  **then**
- 24                     set new iterate starting index  $k_{\text{start}} = k_{\text{start}} + 1$ ;
- 25                 **else**
- 26                     set new iterate starting index  $k_{\text{start}} = \min[k_{\text{pairing}}, k_{\text{unpairing}}]$ ;
- 27                 **end**
- 28                 set new loop index  $i = k_{\text{start}}$ ;
- 29                 re-initialize the temporarily unpaired events index  $k_{\text{pairing}} = N$ ,  $k_{\text{unpairing}} = N$ , temporary empty register set  $A$ , and the number of events in the register  $n_{\text{temp}}$ ;
- 30                 **break**;
- 31             **end**
- 32         **else**
- 33             **if**  $E_j.T_j - t_{\text{start}} \leq \Delta t_{\max}$  **and**  $j < N$  **then**
- 34                 set temporarily unpaired events index:  $k_{\text{unpairing}} = \min[k_{\text{unpairing}}, j]$
- 35             **else**
- 36                 **if**  $n_{\text{temp}} = 1$  **then**
- 37                     set new iterate starting index  $k_{\text{start}} = k_{\text{start}} + 1$ ;
- 38                 **else**
- 39                     set new iterate starting index  $k_{\text{start}} = \min[k_{\text{pairing}}, k_{\text{unpairing}}]$ ;
- 40                 **end**
- 41                 set new loop index  $i = k_{\text{start}}$ ;
- 42                 re-initialize the temporarily unpaired events index  $k_{\text{pairing}} = N$ ,  $k_{\text{unpairing}} = N$ , temporary empty register set  $A$ , and the number of events in the register  $n_{\text{temp}}$ ;
- 43                 **break**;
- 44             **end**
- 45         **end**
- 46     **end**
- 47 **end**
- 48 **end**

---

In the experiment, we adopt the nearest-neighbor pairing algorithm based on [41]. When the program starts running, it takes the first single-count event as the starting point, and then searches backward for the single-count events belonging to other branches with the nearest time intervals. If the time interval between the latest single-count event and the starting point is within the  $t_{\max}$ , then these events from  $N$  different branches will be regarded as a pair, and the unpaired single-count event closest to the starting point will be set as the new starting point. Otherwise, the first unpaired event will be set as the new starting point and repeat the above process when the pairing is not successfully achieved within the specified time interval  $t_{\max}$ .

## S2 KEY MAPPING AND DECOY STATE METHOD

### S2.1 Key mapping

Similar to the time-bin MDI QKD protocol and the MP QKD protocol, in the AMDI QCC protocol, the pairs of early and late pulses that carry users' encoded information are determined based on the rules illustrated in the Fig. S1 below after valid pairing events are obtained:

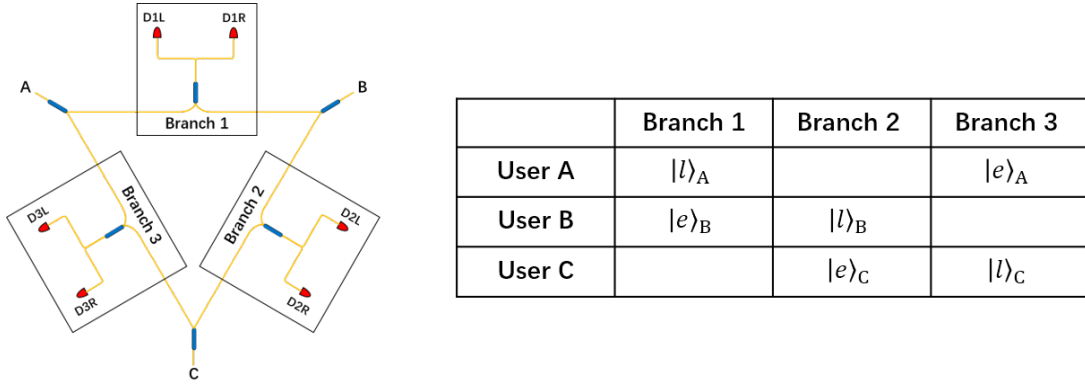


FIG. S1. Three-user AMDI QCC pulse pairing scheme. The table on the right shows the correspondence between the paired pulses of different users and the single-count events from different interferometer branches in the experiment, in which the  $e$  and  $l$  represent the early and late pulse, respectively.

Let the intensities and phases of the early and late pulses for the three users be denoted as  $k_{1,2,3}^{e(l)}$  and  $\varphi_{1,2,3}^{e(l)}$ , respectively. The total intensities of the early and late pulses and their phase differences are defined as  $k_{1,2,3}^{\text{tot}e} = k_{1,2,3}^e + k_{1,2,3}^l$ ,  $\Delta\varphi_{1,2,3} = \varphi_{1,2,3}^l - \varphi_{1,2,3}^e$ , respectively. A pairing event where the total intensities of the three users are  $k_1^{\text{tot}}$ ,  $k_2^{\text{tot}}$ , and  $k_3^{\text{tot}}$  is represented as  $[k_1^{\text{tot}}, k_2^{\text{tot}}, k_3^{\text{tot}}]$ . The methods for determining the Z-basis, X-basis, and their corresponding bit values are as follows:

- Z-basis code: In the experiment, we adopted the with-filter scheme proposed in the literature, which means only the pairing  $([\mu, \mu, \mu])$ —where the total pulse intensity corresponds to the signal state—is selected as a Z-basis event. If  $k^e = \mu$  and  $k^l = o$ , the Z-basis bit value is 0; conversely, if  $k^e = o$  and  $k^l = \mu$ , the Z-basis bit value is 1. A bit error occurs when the Z-basis bit values of all users are not identical. In the without-filter scheme, pairings such as  $[\mu, \mu, \mu]$ ,  $[\mu, \mu, \nu]$ ,  $[\mu, \nu, \mu]$ ,  $[\mu, \nu, \nu]$ ,  $[\nu, \mu, \mu]$ ,  $[\nu, \mu, \nu]$ ,  $[\nu, \nu, \mu]$ , and  $[\nu, \nu, \nu]$  can all be regarded as Z-basis events, which is not adopted in our experiments.
- X-basis code: In the experiment, pairs of  $[2\nu, 2\nu, 2\nu]$  that satisfy  $\theta_{\text{parity}}^X = (\sum_{i=1}^N \theta_i)/\pi \bmod 2 \in \{0, 1\}$  are selected as X-basis events. Let  $r_{1,2,3} \in \{0, 1\}$  denote the response of detector  $D_L$  or  $D_R$  in the three output branches of the interferometer, respectively; then, pairs that satisfy  $r_1 \oplus r_2 \oplus r_3 \oplus \theta_{\text{parity}}^X = 1$  are regarded as X-basis bit error events. In the key generation experiment, for the quantum pulses, the above sifting condition can be modified as  $\theta_{\text{parity}}^X = (\sum_{i=1}^N \theta_i + \theta_{\Delta f}) \bmod 2\pi \in \{\theta_{\min}, \theta_{\min} + \pi\}$ , where the  $\theta_{\Delta f}$  and  $\theta_{\min}$  denote the phase shift introduced by frequency difference and phase drift in the interferometer as mentioned in the text. Besides, for the reference pulses, we keep all  $[2\nu, 2\nu, 2\nu]$  pairs and set the pairs with  $r_1 \oplus r_2 \oplus r_3 = 1$  as error events to obtain the relationship between X-basis QBER and total phase difference, such that we can estimate the phase drift  $\theta_{\min}$ .

## S2.2 Decoy state method

According to the secure key length formula:

$$L_{\min} = \underline{Y}_{111}^Z [1 - H_2(\bar{\epsilon}_{111}^{PZ})] - \max [H_2(e_{AB,AC,BC}^Z)] f n_Z - \log_2 \left( \frac{4}{\epsilon_{\text{cor}}} \right) - 2 \log_2 \left( \frac{2}{\epsilon' \hat{\epsilon}} \right) - 2 \log_2 \left( \frac{1}{2\epsilon_{\text{PA}}} \right). \quad (\text{S2.1})$$

To calculate the key rate, we need to estimate the lower bound of the count  $\underline{Y}_{111}^Z$  and the upper bound of the phase error rate  $\bar{\epsilon}_{111}^{PZ}$  for the single-photon component in the Z-basis. The specific methods are as follows [41]:

- Estimation of statistical fluctuations: Based on the approximate formula for the Chernoff bound given in the literature, given the expected value  $\langle n \rangle$  and failure probability  $\epsilon$ , the upper and lower bound estimates of the real value are respectively:

$$\bar{n} = \langle n \rangle + \frac{\beta}{2} + \sqrt{2\beta\langle n \rangle + \frac{\beta^2}{4}}, \quad \underline{n} = \langle n \rangle - \sqrt{2\beta\langle n \rangle}. \quad (\text{S2.2})$$

Under the same conditions, given the observed value  $n$ , the upper and lower bounds of the expected value  $\langle n \rangle$  are estimated as follows:

$$\overline{\langle n \rangle} = n + \beta + \sqrt{2\beta n + \beta^2} \quad \underline{\langle n \rangle} = \max \left\{ n - \frac{\beta}{2} - \sqrt{2\beta n + \frac{\beta^2}{4}}, 0 \right\}. \quad (\text{S2.3})$$

- Pairing probability: To calculate the expected values of pair count of Z-basis single-photon component and QBER of X-basis single-photon component, it is necessary to calculate the pulse emission probability  $p_{[k_1^{\text{tot}}, k_2^{\text{tot}}, k_3^{\text{tot}}]}$  for different pairing patterns related to the total intensity of early and late pulses:

$$p_{[k_1^{\text{tot}}, k_2^{\text{tot}}, \dots, k_N^{\text{tot}}]} = \frac{1}{p_s^3} \sum_{\substack{k_i^e + k_i^l = k_i^{\text{tot}} \\ \forall i \in \{1, \dots, N\}}} \prod_{i=1}^N p_{k_i^e} p_{k_i^l}, \quad (\text{S2.4})$$

where  $N = 3$  is the number of users, and  $p_s = 1 - \sum_{k_1^e, k_N^l, \dots, k_N^e, k_{N-1}^l \in \{\mu\nu, \nu\mu\}} q_{k_i^e k_{i+1}^e}^{P_i}$  is the correction factor for the filtering scheme, which can be eliminated in the calculation.

- Pair count of Z-basis single-photon component

$$\begin{aligned} \langle Y \rangle_{111}^Z &\geq \frac{e^{-3\mu} p_{[\mu, \mu, \mu]}}{\nu^3 (\mu - \nu)} \left[ \mu^4 \left( e^{3\nu} \frac{\langle n \rangle_{[\nu, \nu, \nu]}}{P_{[\nu, \nu, \nu]}} - e^{2\nu} \frac{\overline{\langle n \rangle}_{[\nu, \nu, o]}}{P_{[\nu, \nu, o]}} - e^{2\nu} \frac{\overline{\langle n \rangle}_{[\nu, o, \nu]}}{P_{[\nu, o, \nu]}} - e^{2\nu} \frac{\overline{\langle n \rangle}_{[o, \nu, \nu]}}{P_{[o, \nu, \nu]}} + e^\nu \frac{\langle n \rangle_{[\nu, \nu, o]}}{P_{[\nu, \nu, o]}} + e^\nu \frac{\langle n \rangle_{[o, \nu, \nu]}}{P_{[o, \nu, \nu]}} \right. \right. \\ &\quad \left. \left. + e^\nu \frac{\langle n \rangle_{[o, o, \nu]}}{P_{[o, o, \nu]}} - \frac{\overline{\langle n \rangle}_{[o, o, o]}}{P_{[o, o, o]}} \right) - \nu^4 \left( e^{3\mu} \frac{\overline{\langle n \rangle}_{[\mu, \mu, \mu]}}{P_{[\mu, \mu, \mu]}} - e^{2\mu} \frac{\langle n \rangle_{[\mu, \mu, o]}}{P_{[\mu, \mu, o]}} - e^{2\mu} \frac{\langle n \rangle_{[\mu, o, \mu]}}{P_{[\mu, o, \mu]}} - e^{2\mu} \frac{\langle n \rangle_{[o, \mu, \mu]}}{P_{[o, \mu, \mu]}} \right. \right. \\ &\quad \left. \left. + e^\mu \frac{\overline{\langle n \rangle}_{[\mu, o, o]}}{P_{[\mu, o, o]}} + e^\mu \frac{\overline{\langle n \rangle}_{[o, \mu, o]}}{P_{[o, \mu, o]}} + e^\mu \frac{\overline{\langle n \rangle}_{[o, o, \mu]}}{P_{[o, o, \mu]}} - \frac{\langle n \rangle_{[o, o, o]}}{P_{[o, o, o]}} \right) \right]. \end{aligned} \quad (\text{S2.5})$$

- Pair count and QBER of X-basis single-photon component

The X-basis single-photon error pair count is:

$$\begin{aligned} \overline{\langle t \rangle}_{111}^X &\leq e^{-6\nu} p_{[2\nu, 2\nu, 2\nu]} \left( e^{6\nu} \frac{\overline{\langle m \rangle}_{[2\nu, 2\nu, 2\nu]}}{P_{[2\nu, 2\nu, 2\nu]}} - e^{4\nu} \frac{\langle n \rangle_{[2\nu, 2\nu, o]}}{2P_{[2\nu, 2\nu, o]}} - e^{4\nu} \frac{\langle n \rangle_{[2\nu, o, 2\nu]}}{2P_{[2\nu, o, 2\nu]}} - e^{4\nu} \frac{\langle n \rangle_{[o, 2\nu, 2\nu]}}{2P_{[o, 2\nu, 2\nu]}} + e^{2\nu} \frac{\overline{\langle n \rangle}_{[2\nu, o, o]}}{2P_{[2\nu, o, o]}} \right. \\ &\quad \left. + e^{2\nu} \frac{\overline{\langle n \rangle}_{[o, 2\nu, o]}}{2P_{[o, 2\nu, o]}} + e^{2\nu} \frac{\overline{\langle n \rangle}_{[o, o, 2\nu]}}{2P_{[o, o, 2\nu]}} - \frac{\langle n \rangle_{[o, o, o]}}{2P_{[o, o, o]}} \right), \end{aligned} \quad (\text{S2.6})$$

where  $\langle m \rangle_{[2\nu, 2\nu, 2\nu]}$  represents the number of X-basis error pairing events. On the other hand, the expected value

of the X-basis single-photon component pair count can be calculated using the corresponding Z-basis count expected value  $\underline{\langle Y \rangle}_{111}^Z$  calculated previously with proportional relation:

$$\frac{\langle Y \rangle_{111}^Z}{\langle Y \rangle_{111}^X} = \frac{\mu^3 e^{-3\mu} p_{[\mu, \mu, \mu]}}{(2\nu e^{-2\nu})^3 p_{[2\nu, 2\nu, 2\nu]}}. \quad (\text{S2.7})$$

After estimating the bound of the true values from the above expected values, the upper bound of the X-basis single-photon QBER can be obtained as  $\bar{e}_{111}^X = \bar{t}_{111}^X / \underline{Y}_{111}^X$ .

- Random sampling formula and Z-basis single-photon phase error rate: Under asymptotic conditions, the Z-basis single-photon phase error rate is identical to the X-basis single-photon bit error rate. However, under conditions of limited data volume, it is necessary to first estimate the corresponding true values based on the previously calculated expected values of each single-photon component, and then calculate  $\bar{e}_{111}^{PZ}$  from these estimates. In the experiment, the random sampling theory used in the literature was adopted, i.e., the upper bound of the true value  $\bar{\chi} = \lambda + \gamma^U(n, k, \lambda, \epsilon)$ , where

$$\gamma^U(n, k, \lambda, \epsilon) = \left[ \frac{(1-2\lambda)AG}{n+k} + \sqrt{\frac{A^2G^2}{(n+k)^2} + 4\lambda(1-\lambda)G} \right] \left( 2 + 2\frac{A^2G}{(n+k)^2} \right)^{-1}, \quad (\text{S2.8})$$

and

$$A = \max\{n, k\}, \quad G = \frac{n+k}{nk} \ln \frac{n+k}{2\pi nk\lambda(1-\lambda)\epsilon^2}. \quad (\text{S2.9})$$

Based on this, the upper bound of the true value of the Z-basis single-photon phase error rate can be finally obtained as:

$$\bar{e}_{111}^{PZ} = \bar{e}_{111}^X + \gamma(\underline{Y}_{111}^Z, \underline{Y}_{111}^X, \bar{e}_{111}^X, \epsilon). \quad (\text{S2.10})$$

### S3 FFT-BASED FREQUENCY DIFFERENCE ESTIMATION

To estimate the frequency difference between users pairwise, in the experiment, we pair the single-count events on the three branches of the interferometer according to the method in MP QKD [51–54], and calculate the X-basis QBER, which is given by the following formula:

$$E_X = \frac{1}{2} - \frac{V_2}{2} \int_{-\infty}^{+\infty} \cos(2\pi\Delta f\Delta t + \omega\Delta t) G(\omega) d\omega = \frac{1-V_2}{2} + \frac{V_2}{2} \left[ 1 - e^{-\sigma^2\Delta t^2/2} \cos(2\pi\Delta f\Delta t) \right], \quad (\text{S2.1})$$

in which the  $V_2$  is visibility of HOM interference;  $\Delta t$  is pairing time interval;  $\omega$  is phase drift rate in fiber; and  $G(\omega)$  is the Gaussian distribution. Since we did not incorporate a long optical fiber,  $\omega$  can be omitted, i.e.,

$$E_X \simeq \frac{1-V_2}{2} + \frac{V_2}{2} [1 - \cos(2\pi\Delta f\Delta t)]. \quad (\text{S2.2})$$

The  $E_X(\Delta t)$  and their spectra obtained by FFT of the three pairs of users are shown in the following Fig. S2. Based on the protocol, the effect of frequency difference on the total relative phase is  $\theta_{\Delta f} = \omega_A(t_1-t_3) + \omega_B(t_2-t_1) + \omega_C(t_3-t_2)$ , which can be rewritten into a form related to the frequency difference between two users:

$$\begin{aligned} \theta_{\Delta f} &= \omega_A(t_1-t_3) + \omega_B(t_2-t_1) + \omega_C(t_3-t_2) = (\omega_A - \omega_B)t_1 + (\omega_B - \omega_C)t_2 + (\omega_C - \omega_A)t_3 \\ &= (\omega_B - \omega_C)(t_2-t_1) + (\omega_C - \omega_A)(t_3-t_1) = \Delta\omega_{BC}\Delta t_{21} + \Delta\omega_{CA}\Delta t_{31}. \end{aligned} \quad (\text{S2.3})$$

Similarly, we can get:

$$\theta_{\Delta f} = \Delta\omega_{CB}\Delta t_{12} + \Delta\omega_{AC}\Delta t_{13} = \Delta\omega_{BA}\Delta t_{21} + \Delta\omega_{AC}\Delta t_{23} = \Delta\omega_{BA}\Delta t_{31} + \Delta\omega_{CB}\Delta t_{32}. \quad (\text{S2.4})$$

After obtaining the frequency estimation values, we calculate the phase compensation values as:

$$\theta_{\Delta f} = \frac{1}{3} [(\Delta\omega_{CB}\Delta t_{12} + \Delta\omega_{AC}\Delta t_{13}) + (\Delta\omega_{BA}\Delta t_{21} + \Delta\omega_{AC}\Delta t_{23}) + (\Delta\omega_{BA}\Delta t_{31} + \Delta\omega_{CB}\Delta t_{32})]. \quad (\text{S2.5})$$

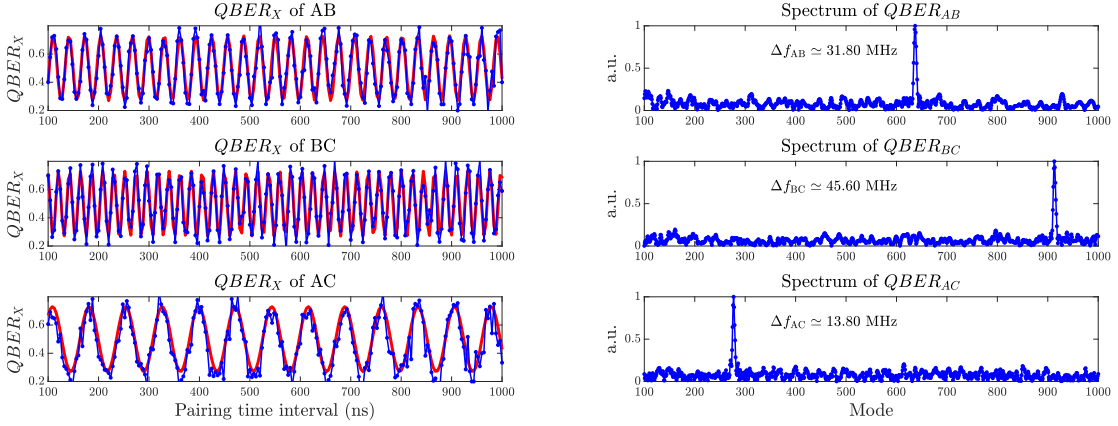


FIG. S2. Two-user X-basis QBERs of reference pulses in the time domain and their spectrum. (a) QBER versus pairing time interval. The blue experimental data points are in good agreement with the red fitting curve, whose HOM interference visibility parameter  $V_2 = 0.46$  and frequency difference parameters are derived from the FFT calculation results. (b) Spectrum of QBERs with the FFT algorithm.

When processing the data, the minimum pairing time interval is selected as the pulse period of 4 ns, and the FFT is performed on the data with pairing intervals ranging from 0.1  $\mu\text{s}$  to 20.1  $\mu\text{s}$ , corresponding to a frequency difference estimation accuracy of about 50 kHz. When analyzing the QBER spectrum, we select the search region for the mode with the maximum amplitude according to the frequency difference measured at the initial moment, which is set to about 1 MHz–125 MHz in the experiment.

## S4 EXPERIMENTAL DATA

### S4.1 Parameters in key rate calculation and simulation

The values of the common parameters used in data processing are as follows:

$\mu$	$\nu$	$p_\mu$	$p_\nu$	$f$	$\varepsilon$	$\Delta t_{\max}$	$e_d$	$p_d$
0.286	0.026	0.1008	0.5398	1.02	$10^{-10}$	3 $\mu\text{s}$	0.01	$4.2 \times 10^{-8}$

TABLE S1. Common parameters in data processing and simulation

The public parameters used in the data processing and simulation are shown in Table S1 above.  $p_\mu$  and  $p_\nu$  represent the average probabilities of the user sending signal states and decoy states, respectively. The overall system loss is calculated based on the intensities and probabilities of the signal and decoy states, and the average single-photon counts of each detector. In the data processing, we filter the data with about 1 ns gate width, such that the dark count rate per pulse is about  $4.2 \times 10^{-8}$ . In the key rate calculation, we uniformly set all security parameters  $\varepsilon_{\text{cor}}$ ,  $\varepsilon'$ ,  $\hat{\varepsilon}$ , and  $\varepsilon_{\text{PA}}$  to  $10^{-10}$ . Besides, more precisely, the data accumulation times under three different loss conditions are about 5003.90 seconds, 20006.85 seconds and 80074.01 seconds, respectively.

When simulating theoretical key rate curves under different experimental conditions, we set the Z-basis QBER to the corresponding measurement values as shown in Table S2. On the other hand, based on the X-basis QBER data, we fit the GHZ-HOM interference visibility for the quantum pulses to be about  $V = 0.182$  at 39.3 dB loss, about  $V = 0.192$  at 48.6 dB, and about  $V = 0.191$  at 59.6 dB loss. Additionally, we set the phase drift rate  $\omega$  in the long fiber to 0, and assume that the frequency difference  $\Delta f = 0$  between users after phase compensation.

### S4.2 Distribution of pair counts by pairing time interval

During data processing in the experiment, we select a maximum pairing interval of  $3 \mu\text{s}$  to reduce the X-basis QBER and increase the key rate. Under three different loss conditions, the pair counts exhibit similar distributions, with average pairing intervals consistently around  $2 \mu\text{s}$ . When the maximum pairing interval is set to infinity, the pairing probability exhibits a maximum point at  $10.35 \mu\text{s}$ ,  $13.72 \mu\text{s}$  and  $20.64 \mu\text{s}$ , with average pairing time intervals of about  $18.79 \mu\text{s}$ ,  $25.26 \mu\text{s}$  and  $35.87 \mu\text{s}$  for 39.3 dB, 48.6 dB and 59.6 dB, respectively.

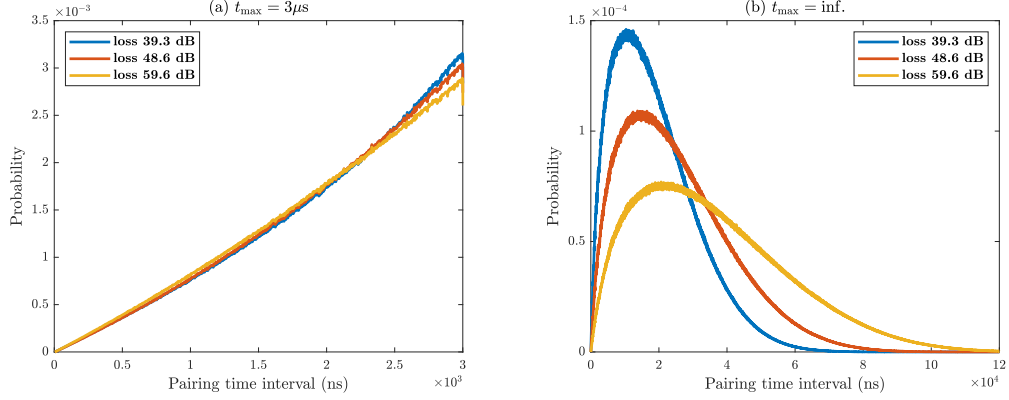


FIG. S3. Distribution of pair counts by pairing time interval. (a)  $t_{\max} = 3 \mu\text{s}$ , (b)  $t_{\max}$  is infinity.

### S4.3 Long-term system stability

The Z-basis QBER and X-basis QBER of the reference pulses with and without adopting frequency and phase drift compensation obtained during about 6 hours of testing are shown in the figure below. Experimental results indicate that the system can maintain stability over long-term data accumulation.

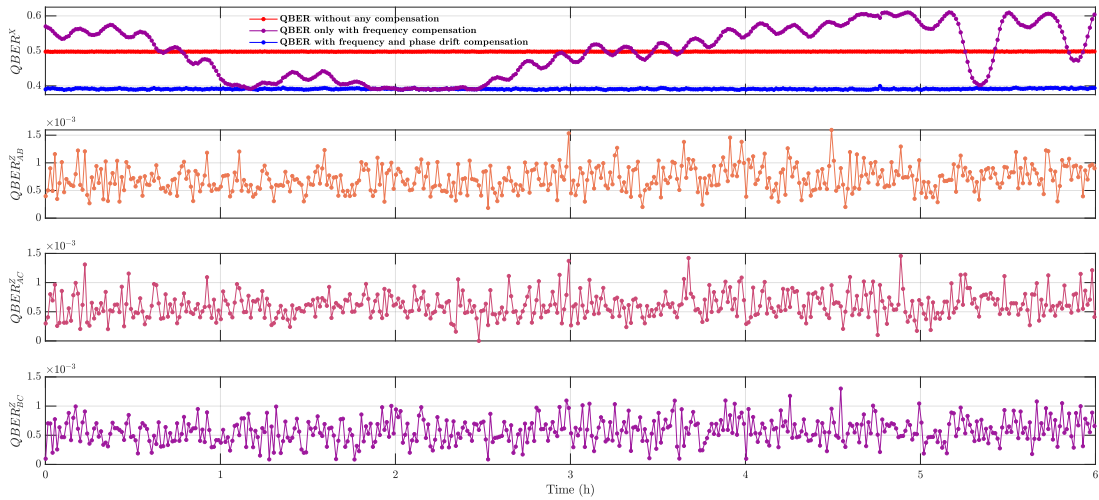


FIG. S4. Stability of QBER. (a) X-basis QBER of reference pulses, (b) Z-basis QBER of users AB, (c) Z-basis QBER of users AC, (d) Z-basis QBER of users BC.

### S4.4 Detailed experimental data

The specific pairing count data under three different loss conditions are shown in the table below. The loss values listed in the table represent user single-node loss including detection-node insertion loss and detection efficiency;  $n_{[\alpha_1, \alpha_2, \alpha_3]}$  denotes the number of pairs whose the sum of the paired early and late pulse intensities for the three user pairs is  $\alpha_1, \alpha_2, \alpha_3$ , respectively; the superscripts  $Z$  and  $X$  respectively indicate the  $Z$ -basis and  $X$ -basis data after pairing and filtering. Especially, we take  $n_{[\mu, \mu, \mu]}$  as  $n_Z$  in the key rate formula S2.1. Besides,  $\overline{\Delta t}$  represents the average pairing time interval,  $L_{\min}$  represents the minimum secure key length, and  $N$  represents the total number of quantum pulses sent by users.

	Att. (dB)	<b>39.3</b>	<b>48.6</b>	<b>59.6</b>
<b>Z-pair counts</b>	$n_{[\mu, \mu, \mu]}$	4536856	5542901	3864918
<b>Total counts</b>	$n_{[\nu, \nu, \nu]}$	585597	701399	484697
	$n_{[o, o, o]}$	0	0	0
	$n_{[\mu, o, o]}$	5	8	2
	$n_{[o, \mu, o]}$	16	10	1
	$n_{[o, o, \mu]}$	14	9	1
	$n_{[\nu, o, o]}$	8	2	0
	$n_{[o, \nu, o]}$	9	4	1
	$n_{[o, o, \nu]}$	9	2	4
	$n_{[o, \mu, \mu]}$	10408	7401	5012
	$n_{[\mu, o, \mu]}$	11045	7962	4507
	$n_{[\mu, \mu, o]}$	10527	6573	4659
	$n_{[o, \nu, \nu]}$	2620	1724	1169
	$n_{[\nu, o, \nu]}$	2827	1947	1129
	$n_{[\nu, \nu, o]}$	2564	1590	1114
	$n_{[\mu, \nu, \nu]}$	1168124	1391282	960283
	$n_{[\nu, \mu, \nu]}$	1142388	1363918	966002
	$n_{[\nu, \nu, \mu]}$	1174619	1447332	983941
	$n_{[\nu, \mu, \mu]}$	2275619	2791992	1946789
	$n_{[\mu, \nu, \mu]}$	2349050	2886105	1958907
	$n_{[\mu, \mu, \nu]}$	2268010	2698297	1907766
	$n_{[\mu, \nu, o]}$	5166	3380	2290
	$n_{[\mu, o, \nu]}$	5584	3918	2266
	$n_{[\nu, \mu, o]}$	5267	3370	2382
	$n_{[\nu, o, \mu]}$	5507	4022	2301
	$n_{[o, \mu, \nu]}$	5073	3529	2454
	$n_{[o, \nu, \mu]}$	5325	3801	2495
	$n_{[2\nu, 2\nu, 2\nu]}$	7740134	9509079	6553982
	$n_{[2\nu, o, o]}$	603	339	172
	$n_{[o, 2\nu, o]}$	944	707	170
	$n_{[o, o, 2\nu]}$	991	741	870
	$n_{[o, 2\nu, 2\nu]}$	841063	1058942	737073
	$n_{[2\nu, o, 2\nu]}$	883452	1172157	716824
	$n_{[2\nu, 2\nu, o]}$	842577	922802	716352
<b>X-pair counts</b>	$n_{[2\nu, 2\nu, 2\nu]}^X$	967876	1189572	820887
<b>Error counts</b>	$E_{[\mu, \mu, \mu]}^{Z_{AB}}$	7778	5242	4353
	$E_{[\mu, \mu, \mu]}^{Z_{AC}}$	7678	5400	2769
	$E_{[\mu, \mu, \mu]}^{Z_{BC}}$	6693	4335	2805
	$E_{[2\nu, 2\nu, 2\nu]}^X$	399992	486164	335669
	$\overline{\Delta t}$ ( $\mu\text{s}$ )	2.078	2.067	2.042
<b>Results</b>	$e_{AB}^Z$ ( $\%_0$ )	1.714	0.946	1.126
	$e_{AC}^Z$ ( $\%_0$ )	1.692	0.974	0.716
	$e_{BC}^Z$ ( $\%_0$ )	1.475	0.782	0.726
	$\frac{Y_{111}^Z}{e_{111}^Z}$	$1.951 \times 10^6$	$2.391 \times 10^6$	$1.643 \times 10^6$
	$\frac{P_{111}^Z}{e_{111}^Z}$	0.3528	0.3232	0.3413
	$L_{\min}$	$3.932 \times 10^4$	$1.571 \times 10^5$	$7.139 \times 10^4$
	$L_{\min}/N$	$3.940 \times 10^{-8}$	$3.937 \times 10^{-8}$	$4.470 \times 10^{-9}$

TABLE S2: Detailed results of the AMDI QCC experiment

\* [xiaosong.ma@nju.edu.cn](mailto:xiaosong.ma@nju.edu.cn)

- [1] S. Wehner, D. Elkouss, and R. Hanson, Quantum internet: A vision for the road ahead, *Science* **362**, eaam9288 (2018).
- [2] H. J. Kimble, The quantum internet, *Nature* **453**, 1023 (2008).
- [3] C. H. Bennett and G. Brassard, Quantum cryptography: Public key distribution and coin tossing, in *Proceedings of IEEE International Conference on Computers, Systems, and Signal Processing* (IEEE, New York, 1984) p. 175–179.
- [4] A. K. Ekert, Quantum cryptography based on bell’s theorem, *Phys. Rev. Lett.* **67**, 661 (1991).
- [5] N. Gisin, G. Ribordy, W. Tittel, and H. Zbinden, Quantum cryptography, *Rev. Mod. Phys.* **74**, 145 (2002).
- [6] V. Scarani, H. Bechmann-Pasquinucci, N. J. Cerf, M. Dušek, N. Lütkenhaus, and M. Peev, The security of practical quantum key distribution, *Rev. Mod. Phys.* **81**, 1301 (2009).
- [7] F. Xu, X. Ma, Q. Zhang, H.-K. Lo, and J.-W. Pan, Secure quantum key distribution with realistic devices, *Rev. Mod. Phys.* **92**, 025002 (2020).
- [8] S. Pirandola, U. L. Andersen, L. Banchi, M. Berta, D. Bunandar, R. Colbeck, D. Englund, T. Gehring, C. Lupo, C. Ottaviani, J. L. Pereira, M. Razavi, J. S. Shaari, M. Tomamichel, V. C. Usenko, G. Vallone, P. Villoresi, and P. Wallden, Advances in quantum cryptography, *Adv. Opt. Photon.* **12**, 1012 (2020).
- [9] W.-Y. Hwang, Quantum key distribution with high loss: Toward global secure communication, *Phys. Rev. Lett.* **91**, 057901 (2003).
- [10] X.-B. Wang, Beating the photon-number-splitting attack in practical quantum cryptography, *Phys. Rev. Lett.* **94**, 230503 (2005).
- [11] H.-K. Lo, X. Ma, and K. Chen, Decoy state quantum key distribution, *Phys. Rev. Lett.* **94**, 230504 (2005).
- [12] A. Acín, N. Brunner, N. Gisin, S. Massar, S. Pironio, and V. Scarani, Device-independent security of quantum cryptography against collective attacks, *Phys. Rev. Lett.* **98**, 230501 (2007).
- [13] S. L. Braunstein and S. Pirandola, Side-channel-free quantum key distribution, *Phys. Rev. Lett.* **108**, 130502 (2012).
- [14] H.-K. Lo, M. Curty, and B. Qi, Measurement-device-independent quantum key distribution, *Phys. Rev. Lett.* **108**, 130503 (2012).
- [15] M. Lucamarini, Z. L. Yuan, J. F. Dynes, and A. J. Shields, Overcoming the rate–distance limit of quantum key distribution without quantum repeaters, *Nature* **557**, 400 (2018).
- [16] Y.-M. Xie, Y.-S. Lu, C.-X. Weng, X.-Y. Cao, Z.-Y. Jia, Y. Bao, Y. Wang, Y. Fu, H.-L. Yin, and Z.-B. Chen, Breaking the rate-loss bound of quantum key distribution with asynchronous two-photon interference, *PRX Quantum* **3**, 020315 (2022).
- [17] P. Zeng, H. Zhou, W. Wu, and X. Ma, Mode-pairing quantum key distribution, *Nature Communications* **13**, 3903 (2022).
- [18] J. Yin, Y.-H. Li, S.-K. Liao, M. Yang, Y. Cao, L. Zhang, J.-G. Ren, W.-Q. Cai, W.-Y. Liu, S.-L. Li, R. Shu, Y.-M. Huang, L. Deng, L. Li, Q. Zhang, N.-L. Liu, Y.-A. Chen, C.-Y. Lu, X.-B. Wang, F. Xu, J.-Y. Wang, C.-Z. Peng, A. K. Ekert, and J.-W. Pan, Entanglement-based secure quantum cryptography over 1,120 kilometres, *Nature* **582**, 501 (2020).
- [19] Y.-A. Chen, Q. Zhang, T.-Y. Chen, W.-Q. Cai, S.-K. Liao, J. Zhang, K. Chen, J. Yin, J.-G. Ren, Z. Chen, S.-L. Han, Q. Yu, K. Liang, F. Zhou, X. Yuan, M.-S. Zhao, T.-Y. Wang, X. Jiang, L. Zhang, W.-Y. Liu, Y. Li, Q. Shen, Y. Cao, C.-Y. Lu, R. Shu, J.-Y. Wang, L. Li, N.-L. Liu, F. Xu, X.-B. Wang, C.-Z. Peng, and J.-W. Pan, An integrated space-to-ground quantum communication network over 4,600 kilometres, *Nature* **589**, 214 (2021).
- [20] W. Li, L. Zhang, H. Tan, Y. Lu, S.-K. Liao, J. Huang, H. Li, Z. Wang, H.-K. Mao, B. Yan, Q. Li, Y. Liu, Q. Zhang, C.-Z. Peng, L. You, F. Xu, and J.-W. Pan, High-rate quantum key distribution exceeding 110 mb s<sup>-1</sup>, *Nature Photonics* **17**, 416 (2023).
- [21] Y. Liu, W.-J. Zhang, C. Jiang, J.-P. Chen, C. Zhang, W.-X. Pan, D. Ma, H. Dong, J.-M. Xiong, C.-J. Zhang, H. Li, R.-C. Wang, J. Wu, T.-Y. Chen, L. You, X.-B. Wang, Q. Zhang, and J.-W. Pan, Experimental twin-field quantum key distribution over 1000 km fiber distance, *Phys. Rev. Lett.* **130**, 210801 (2023).
- [22] S. Wengerowsky, S. K. Joshi, F. Steinlechner, H. Hübel, and R. Ursin, An entanglement-based wavelength-multiplexed quantum communication network, *Nature* **564**, 225 (2018).
- [23] S. K. Joshi, D. Aktas, S. Wengerowsky, M. Lončarić, S. P. Neumann, B. Liu, T. Scheidl, G. C. Lorenzo, Željko Samec, L. Kling, A. Qiu, M. Razavi, M. Stipčević, J. G. Rarity, and R. Ursin, A trusted node-free eight-user metropolitan quantum communication network, *Science Advances* **6**, eaba0959 (2020).
- [24] W. Wen, Z. Chen, L. Lu, W. Yan, W. Xue, P. Zhang, Y. Lu, S. Zhu, and X.-S. Ma, Realizing an entanglement-based multiuser quantum network with integrated photonics, *Phys. Rev. Appl.* **18**, 024059 (2022).
- [25] W. Yan, X. Zheng, W. Wen, L. Lu, Y. Du, Y.-Q. Lu, S. Zhu, and X.-S. Ma, A measurement-device-independent quantum key distribution network using optical frequency comb, *npj Quantum Information* **11**, 97 (2025).
- [26] S. Bose, V. Vedral, and P. L. Knight, Multiparticle generalization of entanglement swapping, *Phys. Rev. A* **57**, 822 (1998).
- [27] K. Chen and H.-K. Lo, Multipartite quantum cryptographic protocols with noisy ghz states, *Quantum Information and Computation* **7** (2007).
- [28] G. Murta, F. Grasselli, H. Kampermann, and D. Bruß, Quantum conference key agreement: A review, *Advanced Quantum Technologies* **3**, 2000025 (2020).
- [29] R. Augusiak and P. Horodecki, Multipartite secret key distillation and bound entanglement, *Phys. Rev. A* **80**, 042307 (2009).
- [30] G. Carrara, H. Kampermann, D. Bruß, and G. Murta, Genuine multipartite entanglement is not a precondition for secure conference key agreement, *Phys. Rev. Res.* **3**, 013264 (2021).

- [31] S. Das, S. Bäuml, M. Winczewski, and K. Horodecki, Universal limitations on quantum key distribution over a network, *Phys. Rev. X* **11**, 041016 (2021).
- [32] M. Epping, H. Kampermann, C. Macchiavello, and D. Bruß, Multi-partite entanglement can speed up quantum key distribution in networks, *New Journal of Physics* **19**, 093012 (2017).
- [33] F. Grasselli, H. Kampermann, and D. Bruß, Finite-key effects in multipartite quantum key distribution protocols, *New Journal of Physics* **20**, 113014 (2018).
- [34] Y. Fu, H.-L. Yin, T.-Y. Chen, and Z.-B. Chen, Long-distance measurement-device-independent multiparty quantum communication, *Phys. Rev. Lett.* **114**, 090501 (2015).
- [35] F. Grasselli, H. Kampermann, and D. Bruß, Conference key agreement with single-photon interference, *New Journal of Physics* **21**, 123002 (2019).
- [36] S. Zhao, P. Zeng, W.-F. Cao, X.-Y. Xu, Y.-Z. Zhen, X. Ma, L. Li, N.-L. Liu, and K. Chen, Phase-matching quantum cryptographic conferencing, *Phys. Rev. Appl.* **14**, 024010 (2020).
- [37] X.-Y. Cao, J. Gu, Y.-S. Lu, H.-L. Yin, and Z.-B. Chen, Coherent one-way quantum conference key agreement based on twin field, *New Journal of Physics* **23**, 043002 (2021).
- [38] X.-Y. Cao, Y.-S. Lu, Z. Li, J. Gu, H.-L. Yin, and Z.-B. Chen, High key rate quantum conference key agreement with unconditional security, *IEEE Access* **9**, 128870 (2021).
- [39] J.-L. Bai, Y.-M. Xie, Z. Li, H.-L. Yin, and Z.-B. Chen, Post-matching quantum conference key agreement, *Optics Express* **30**, 28865 (2022).
- [40] G. Carrara, G. Murta, and F. Grasselli, Overcoming fundamental bounds on quantum conference key agreement, *Phys. Rev. Appl.* **19**, 064017 (2023).
- [41] Y.-S. Lu, H.-L. Yin, Y.-M. Xie, Y. Fu, and Z.-B. Chen, Repeater-like asynchronous measurement-device-independent quantum conference key agreement, *Reports on Progress in Physics* **88**, 067901 (2025).
- [42] Y.-M. Xie, Y.-S. Lu, Y. Fu, H.-L. Yin, and Z.-B. Chen, Multi-field quantum conferencing overcomes the network capacity limit, *Communications Physics* **7**, 410 (2024).
- [43] M. Proietti, J. Ho, F. Grasselli, P. Barrow, M. Malik, and A. Fedrizzi, Experimental quantum conference key agreement, *Science Advances* **7**, eabe0395 (2021).
- [44] A. Pickston, J. Ho, A. Ulibarrena, F. Grasselli, M. Proietti, C. L. Morrison, P. Barrow, F. Graffitti, and A. Fedrizzi, Conference key agreement in a quantum network, *npj Quantum Information* **9**, 82 (2023).
- [45] S. Pirandola, R. Laurenza, C. Ottaviani, and L. Banchi, Fundamental limits of repeaterless quantum communications, *Nature Communications* **8**, 15043 (2017).
- [46] K.-X. Yang, Y.-L. Mao, H. Chen, X. Dong, J. Zhu, J. Wu, and Z.-D. Li, Experimental measurement-device-independent quantum conference key agreement, *Phys. Rev. Lett.* **133**, 210803 (2024).
- [47] Y. Du, Y. Liu, C. Yang, X. Zheng, S. Zhu, and X.-S. Ma, Experimental Measurement-Device-Independent Quantum Cryptographic Conferencing, *Phys. Rev. Lett.* **134**, 040802 (2025).
- [48] H.-T. Zhu, Y. Huang, H. Liu, P. Zeng, M. Zou, Y. Dai, S. Tang, H. Li, L. You, Z. Wang, Y.-A. Chen, X. Ma, T.-Y. Chen, and J.-W. Pan, Experimental Mode-Pairing Measurement-Device-Independent Quantum Key Distribution without Global Phase Locking, *Phys. Rev. Lett.* **130**, 030801 (2023).
- [49] L. Zhou, J. Lin, Y.-M. Xie, Y.-S. Lu, Y. Jing, H.-L. Yin, and Z. Yuan, Experimental Quantum Communication Overcomes the Rate-Loss Limit without Global Phase Tracking, *Phys. Rev. Lett.* **130**, 250801 (2023).
- [50] H.-T. Zhu, Y. Huang, W.-X. Pan, C.-W. Zhou, J. Tang, H. He, M. Cheng, X. Jin, M. Zou, S. Tang, X. Ma, T.-Y. Chen, and J.-W. Pan, Field test of mode-pairing quantum key distribution, *Optica* **11**, 883 (2024).
- [51] L. Zhang, W. Li, J. Pan, Y. Lu, W. Li, Z.-P. Li, Y. Huang, X. Ma, F. Xu, and J.-W. Pan, Experimental Mode-Pairing Quantum Key Distribution Surpassing the Repeaterless Bound, *Physical Review X* **15**, 021037 (2025).
- [52] S.-F. Shao, L. Zhou, J. Lin, M. Minder, C. Ge, Y.-M. Xie, A. Shen, Z. Yan, H.-L. Yin, and Z. Yuan, High-Rate Measurement-Device-Independent Quantum Communication without Optical Reference Light, *Physical Review X* **15**, 021066 (2025).
- [53] Y.-F. Lu, Y.-Y. Zhou, Y.-Y. Guo, X.-H. Li, X.-L. Jiang, Y. Wang, Y. Zhou, J.-J. Li, C. Zhou, H.-W. Li, L.-J. Zhou, and W.-S. Bao, Experimental Frequency-Comb-Based Mode-Pairing Quantum Key Distribution Beyond the Rate-Loss Limit [10.48550/arXiv.2505.09223](https://arxiv.org/abs/2505.09223) (2025), arXiv:2505.09223 [quant-ph].
- [54] W. Li, L. Zhang, Y. Lu, Z.-P. Li, C. Jiang, Y. Liu, J. Huang, H. Li, Z. Wang, X.-B. Wang, Q. Zhang, L. You, F. Xu, and J.-W. Pan, Twin-Field Quantum Key Distribution without Phase Locking, *Phys. Rev. Lett.* **130**, 250802 (2023).
- [55] See Supplemental Material for the detailed analysis of the frequency difference estimation method interference (Sec. S3).
- [56] T. J. Kippenberg, A. L. Gaeta, M. Lipson, and M. L. Gorodetsky, Dissipative Kerr solitons in optical microresonators, *Science* **361**, eaan8083 (2018).
- [57] M. Kues, C. Reimer, J. M. Lukens, W. J. Munro, A. M. Weiner, D. J. Moss, and R. Morandotti, Quantum optical microcombs, *Nature Photonics* **13**, 170 (2019).
- [58] B. Shen, L. Chang, J. Liu, H. Wang, Q.-F. Yang, C. Xiang, R. N. Wang, J. He, T. Liu, W. Xie, J. Guo, D. Kinghorn, L. Wu, Q.-X. Ji, T. J. Kippenberg, K. Vahala, and J. E. Bowers, Integrated turnkey soliton microcombs, *Nature* **582**, 365 (2020).
- [59] G. Moille, J. Stone, M. Chojnacky, R. Shrestha, U. A. Javid, C. Menyuk, and K. Srinivasan, Kerr-induced synchronization of a cavity soliton to an optical reference, *Nature* **624**, 267 (2023).
- [60] L. Huang, W. Wang, F. Wang, Y. Wang, C. Zou, L. Tang, B. E. Little, W. Zhao, Z. Han, J. Yang, G. Wang, W. Chen, and W. Zhang, Massively parallel Hong-Ou-Mandel interference based on independent soliton microcombs, *Science Advances* **11**, eadq8982 (2025).

- [61] W. Yan, Y. Hu, Y. Du, K. Wang, Y.-Q. Lu, S. Zhu, and X.-S. Ma, Ten-channel Hong–Ou–Mandel interference between independent optical combs, *Chinese Optics Letters* **23**, 042701 (2025).
- [62] C. Wang, M. Zhang, X. Chen, M. Bertrand, A. Shams-Ansari, S. Chandrasekhar, P. Winzer, and M. Lončar, Integrated lithium niobate electro-optic modulators operating at CMOS-compatible voltages, *Nature* **562**, 101 (2018).
- [63] F. Grünenfelder, A. Boaron, G. V. Resta, M. Perrenoud, D. Rusca, C. Barreiro, R. Houlmann, R. Sax, L. Stasi, S. El-Khoury, E. Hänggi, N. Bosshard, F. Bussières, and H. Zbinden, Fast single-photon detectors and real-time key distillation enable high secret-key-rate quantum key distribution systems, *Nature Photonics* **17**, 422 (2023).
- [64] M. Zou, B.-C. Li, S. Zhao, Y. Mao, D. Qin, X. Jiang, T.-Y. Chen, and J.-W. Pan, Experimental phase-matching quantum cryptographic conferencing in symmetric and asymmetric fiber channels, *Phys. Rev. Lett.* **136**, 020801 (2026).